THE ASTROPHYSICAL JOURNAL, 266:415–424, 1983 March 1

AN ANALYSIS OF THE REFLECTION SPECTRUM OF JUPITER FROM 1500 Å TO 1740 Å

G. RANDALL GLADSTONE AND YUK L. YUNG
Division of Geological and Planetary Sciences, California Institute of Technology
Received 1982 April 5; accepted 1982 August 24

ABSTRACT

A study is made of the UV reflection spectrum of Jupiter as measured by the *International Ultraviolet Explorer*. Detailed modeling reveals the mixing ratios of C_2H_2, C_2H_6, and C_4H_2 to be $(1.0 \pm 0.1) \times 10^{-7}$, $(6.6 \pm 5.3) \times 10^{-6}$, and $(2.9 \pm 2.0) \times 10^{-10}$, respectively, in the pressure region between ~ 3 and 40 mbar. Upper limits in this pressure region for the mixing ratios of C_2H_4 and NH_3 were determined to be $(3.9^{+4.9}_{-3.9}) \times 10^{-10}$ and $(4.2^{+6.7}_{-4.2}) \times 10^{-9}$, respectively. An upper limit to the optical depth of dust above the tropopause, assuming it is well mixed, is $0.2^{+0.3}_{-0.2}$, and an upper limit on the dayglow emission by the Lyman bands of H_2 is $1.4^{+2.4}_{-1.4}$ kR. Comparison with *Voyager* results suggests that the scale height of C_2H_2 in the region 150–10 mbar is approximately twice that of the bulk atmosphere, consistent with the *IUE* observation of cosine-like limb darkening in the north-south direction on Jupiter in this spectral range. These results are of use in the photochemical modeling of the upper atmosphere of Jupiter.

Subject headings: planets: abundances — planets: atmospheres — planets: Jupiter — planets: spectra — ultraviolet: spectra

I. INTRODUCTION

Solar ultraviolet light in the range from 1500 Å to 1740 Å penetrates the atmosphere of Jupiter to a pressure of ~ 10–30 mbar. This region is located between two and three scale heights above the tropopause (at ~ 150 mbar). The principal absorbing gases expected in this region are C_2H_2 and C_2H_6. Possible minor absorption may be present due to C_4H_2 and C_2H_4. Although these last two gases have not been detected spectroscopically, their presence is predicted by photochemical models of Jupiter, and they have large absorption cross sections in this spectral range. Methane is not an important absorber at wavelengths above 1500 Å. Although its mixing ratio falls rapidly with height above the tropopause due to photodissociation, NH_3 may also affect the spectrum, especially at the longer wavelengths. Other gases, such as CH_3C_2H, C_3H_8, PH_3, and H_2S may also have a marginal effect on the spectrum if they are present in the region, but they are not considered here. In most recent models of the reflection spectra of Jupiter at longer wavelengths (0.3–1 μm) it has been found necessary to include a haze layer above the cloud deck at ~ 500 mbar. This haze extends up to ~ 150 mbar or possibly higher (Sato and Hansen 1979; West 1981). Also complicating the spectrum is the presence of dayglow emission from the H_2 Lyman bands at a much higher altitude.

In this study, we have modeled the reflection spectrum in an attempt to determine the mixing ratios of the major gases C_2H_2 and C_2H_6, obtain upper limits to the mixing ratios of the minor gases C_2H_4, C_4H_2, and NH_3, determine the amount of dust (if any) in the stratosphere, and deduce the intensity of the H_2 Lyman band dayglow emission. The derived mixing ratios and upper limits are useful in constraining photochemical models of the upper atmosphere of Jupiter. They may also be compared with mixing ratios determined from infrared spectra, such as the IRIS instruments on *Voyager 1* and *Voyager 2*. One advantage of analyzing UV absorption spectra to obtain mixing ratios is that the results are not sensitive to the temperature profile. We are also able to obtain some constraints on the scale heights of the major absorbers (C_2H_2 and C_2H_6) at ~ 10 mbar.

In § II we discuss the data and the model parameters associated with the *International Ultraviolet Explorer* (*IUE*). In § III the model parameters associated with the atmosphere of Jupiter are described, along with the homogeneous and inhomogeneous models that were used. In § IV we present the results of the modeling calculations and compare these with the results of others. Our conclusions are presented in § V.

II. DATA AND *IUE* MODEL PARAMETERS

The spectrum we are modeling is a sum of eleven 15-minute spectra taken of Jupiter between 1978 December and 1979 June with the *IUE* (Clarke, Moos, and Feldman 1982). The spectra were taken at low resolution with the large aperture of the short-wavelength prime camera centered on Jupiter. The resulting spectral resolution was 10 Å full width half-maximum (FWHM). This spectrum is shown in Figure 1*a*, along with a scaled solar spectrum (Mount, Rottman, and Timothy 1980) degraded to *IUE* resolution. Also shown in this figure above 1695 Å is a spectrum which is the sum of three 5-minute spectra. Below 1500 Å the signal is too small to be modeled, while above 1740 Å

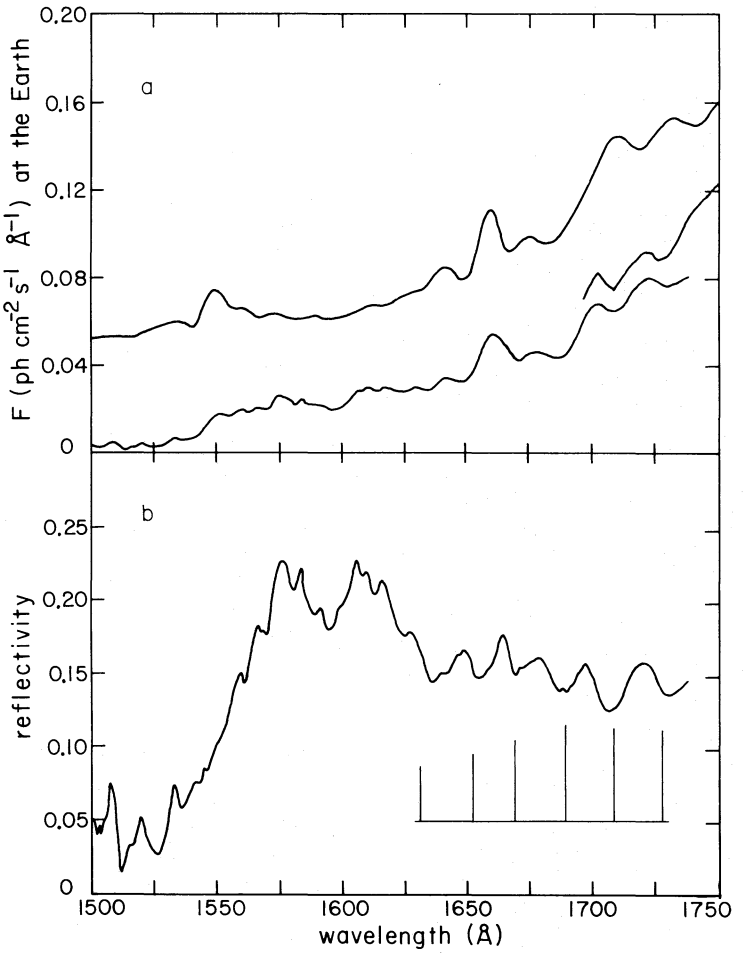

FIG. 1.—(*a*) *Lower line 1500–1740 Å;* sum of eleven 15-minute exposures of Jupiter taken with the *IUE* between 1978 December and 1979 June by Clarke, Moos, and Feldman (1982). *Lower line 1700–1750 Å;* sum of three 5-minute exposures taken between 1980 May and July. *Upper line;* solar spectrum of Mount, Rottman, and Timothy (1980) degraded by *IUE* resolution. The upper line scale is shifted upward by 0.04 and is the flux that would be observed by the *IUE* if the backscattered reflectivity of Jupiter were 0.2. (*b*) The observed UV reflectivity of Jupiter from 1500–1740 Å using the data in Fig. 1*a*. The major absorption features of C_2H_2 longward of 1625 Å are indicated (see also Fig. 7).

scattered light begins to be a problem in the *IUE* (Clarke, Moos, and Feldman 1982). We thus restrict our modeling to within these limits.

As seen from the *IUE*, the phase angle of Jupiter is always less than 11°. In our models we consider the phase angle to be 0°. The error introduced by this approximation is less than 2% as long as the single-scattering albedo of the atmosphere is below 0.8. The footprint of the large aperture [subtending a solid angle of 175 arcsec^2 or 4.11(−9) sr] on Jupiter was such that the average solar zenith angle within it was ~20°. The flux received by the *IUE* from Jupiter is given by

$$F_\oplus = \omega\left(\frac{pF_\odot}{\pi R^2} + \frac{10^9}{4\pi} I_{\text{dayglow}}\right), \qquad (1)$$

where $\omega \equiv$ the solid angle subtended by the *IUE* aperture = 4.11(−9) sr, $p \equiv$ the backscattering reflectivity of Jupiter averaged over the footprint of the *IUE* aperture on the planet, $F_\odot \equiv$ the solar flux at 1 AU (taken from Mount, Rottman, and Timothy 1980), $R \equiv$ the Sun-Jupiter distance in AU = 5.203, and $I_{\text{dayglow}} \equiv$ the H_2 Lyman band emission in kilorayleighs (1 kR = 10^9 photons cm^{-2} s^{-1}). We approximate p with I/F at $\mu = \mu_0 = \cos 20°$, $\varphi = \varphi_0 = 180°$ (where μ is the cosine of the local zenith angle and φ is the azimuth angle). The variation of the observed p with wavelength is shown in Figure 1*b*, along with identification of some of the major absorption bands of C_2H_2.

$F_\oplus$ is calculated at 1 Å intervals (both the solar fluxes and the H_2 band intensities used are at 1 Å resolution) and is then degraded to *IUE* resolution for comparison with the observed spectrum. We model $F_\oplus$ rather than the observed p reflectivity for the following reason. Modeling of $F_\oplus$ requires only one smoothing of the model calculations to simulate the data. To model the observed p we would need to smooth the calculations a second time, either before or after division by the scaled solar fluxes. This would degrade the spectrum unnecessarily, reducing the amount of information

contained in it and adding artifacts from the solar spectrum.

Degrading the calculated model spectrum to *IUE* resolution requires knowledge of the *IUE* instrument function. Since Jupiter is a diffuse source, the instrument function is a convolution of the large aperture with the grating function and then with the analyzing aperture. The dimensions of the large aperture have recently been redetermined by Panek (1981). This aperture is the major source of dispersion, having a FWHM of 9.6 ± 0.3 Å. The grating function is assumed to be a Gaussian with a FWHM of 4.2 Å. The analyzing aperture we consider to be a delta function, since exposures are read out pixel by pixel, which introduces no additional dispersion. The resulting instrument function we calculate has a FWHM of 9.6 Å and is shown in Figure 2. By applying this smoothing function to our calculated spectra we obtain a reasonably good fit to the *IUE* spectrum. There remains a slight difference in resolution which may be a result of the error in the aperture dimensions, the stacking of the *IUE* spectra, or possibly the inhomogeneity of the atmosphere, as we will show in §§ III and IV.

III. JUPITER MODEL PARAMETERS

From the previous section it is clear that the only Jupiter-related parameters necessary for the modeling of the *IUE* spectrum are the backscattering reflectivity averaged over the footprint of the *IUE* aperture on Jupiter, which we approximate by I/F ($\mu = \mu_0 = \cos 20°$, $\varphi = \varphi_0 = 180°$), and the amount of emission in the H_2 Lyman bands. We use the results of Yung *et al.* (1982) for the spectral shape of the H_2 Lyman bands and assume that the emission is excited by 100 eV electrons.

As a first approximation, we consider the atmosphere of Jupiter to be homogeneous, i.e., the mixing ratios of all the scatterers and absorbers are assumed to be constant throughout the atmosphere. The only scatterers in our model are H_2, He, and "dust." For simplicity, we assume that the dust has a Rayleigh phase function, as do the gases. This is, of course, not a very realistic assumption, but it allows the dust to make a small contribution to the scattering. The main purpose of including dust is to test the need for a continuum absorber. The H_2 volume mixing ratio is held constant at 89% ($f_{H_2} = 0.89$), so that H_2 does most of the scattering. The cross sections for Rayleigh scattering by H_2 were taken from Ford and Browne (1973). We hold f_{He} constant at 0.11 and take the scattering cross sections to be 0.1 times those of the H_2, based on relative polarizabilities. Since He accounts for at most ~1% of the scattering, this assumption will not greatly affect the model results. The value of f_{dust} is allowed to vary, and the total cross section is assumed to be constant at 1×10^{-16} cm^2. The single-scattering albedo of the dust we use is that of Sato and Hansen (1979) which has the form

$$\varpi_{dust} = \frac{1}{1 + 10^{-6.4\lambda + 1.7}}, \qquad (2)$$

with λ in microns. This gives $\varpi_{dust} = 0.18$ at 1650 Å, so that the particles are very dark in the UV. This formula was derived for wavelengths above 3000 Å, and it is probable that it does not hold too well at the wavelengths we are considering. However, any errors in ϖ_{dust} can be adjusted for in the derived f_{dust} if necessary.

The absorbers considered in the model (besides the dust) are C_2H_2, C_2H_6, C_4H_2, C_2H_4, and NH_3, in roughly the order of their importance. The cross sections for these absorbers are taken from Nakayama and

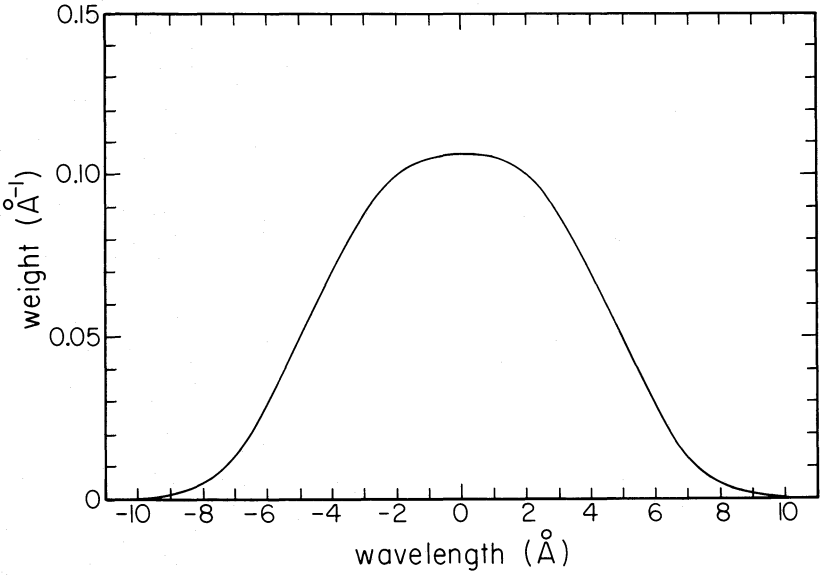

FIG. 2.—The instrument function for the SWP camera of the *IUE* for an extended source observed under low dispersion with the large aperture.

Watanabe (1964), Mount and Moos (1978), Okabe (1981), Zelikoff and Watanabe (1953), and Watanabe (1954), respectively.

We also assume that the atmosphere is infinite. This is clearly not true for the real atmosphere, since below the tropopause the mixing ratios of all of the hydrocarbons (except CH_4) will decrease rapidly. The reason for this is that these gases are created photochemically in the stratosphere and are not in thermodynamic equilibrium. Once they pass below the tropopause they will be mixed rapidly down to levels where they can be destroyed by pyrolysis. However, if the total optical depth at the tropopause is $\gtrsim 3$, and the single-scattering albedo is less than ~ 0.8, then any structure below the tropopause will have less than a 10% effect on the backscattered reflectivity. As we will see, this is indeed the case.

For an infinite, homogeneous atmosphere, the only remaining parameter that can modify I/F is the single-scattering albedo, ϖ_0. For a mixture of scattering and absorbing gases, we define ϖ_0 as

$$\varpi_0 = \left(1 + \frac{\sum f_a \sigma_a}{\sum f_s \sigma_s}\right)^{-1}, \quad (3)$$

where $f_a \equiv$ absorber mixing ratio at 10 mbar, $f_s \equiv$ scatterer mixing ratio at 10 mbar, $\sigma_a \equiv$ absorber cross section, and $\sigma_s \equiv$ scatterer cross section. The choice of reference level is arbitrary, and $P = 10$ mbar is used because for most of the spectral range considered it is approximately the level at which the total optical depth is 0.5.

A plot of I/F versus ϖ_0 for a homogeneous, infinite atmosphere is shown in Figure 3. The curves in this figure were calculated using a ten-stream Feautrier radiative transfer program (see Gladstone 1982). We find that the empirical function

$$I/F = -0.1854 \ln (1 - \varpi_0) \quad (4)$$

represents the true I/F to within 1% for $\varpi_0 < 0.95$.

To produce a model fit to the observed spectrum we proceed as follows. First, a guess is made for the volume mixing ratios of the absorbing gases and dust, and for the intensity of the Lyman band emission. Next, we calculate $F_\oplus$ at 1 Å intervals via equations (3), (4), and (1). This model spectrum is then smoothed using the *IUE* aperture function of § II (see Fig. 2) and compared to the observed spectrum between 1500 Å and 1740 Å. The model parameters are then updated, and the cycle is repeated until the model spectrum is a least squares approximation of the observed spectrum.

Although the homogeneous models provide a fairly good fit to the observed spectrum, we also wanted to explore cases that were more like the real Jupiter, that is to say, inhomogeneous. To accomplish this we add an extra parameter, the ratio of scatterer to absorber scale heights. The reason for the difference between the two scale heights is that the main absorbers C_2H_2 and C_2H_6 are produced in the stratosphere and are being mixed down until they pass through the tropopause. Their scale heights are determined by the atmospheric eddy diffusion profile and their chemical lifetimes, and they are likely to be different from the scale height of the bulk (H_2) atmosphere. For a range of eddy diffusion coefficients at the tropopause between 1×10^3 and 1×10^4 cm^2 s^{-1}, we expect that the mixing ratios of both C_2H_2 and C_2H_6 will increase with height, i.e., the ratio of scatterer to absorber scale heights, $H_s/H_a < 1$. On the other hand, absorbers such as NH_3 and dust are expected to have

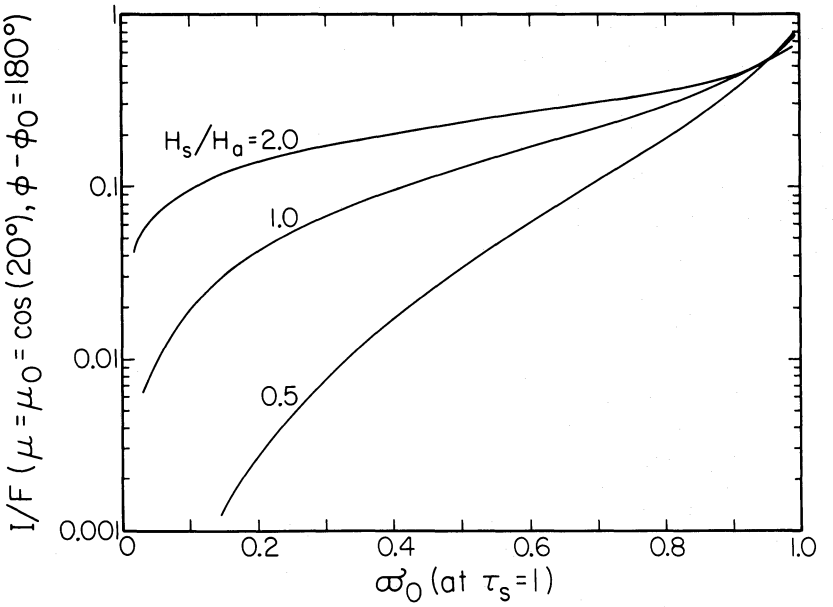

FIG. 3.—Backscattered reflectivity vs. the single-scattering albedo at the level where $\tau_s = 1$, for the cases in which the ratio of scatterer to absorber scale heights, H_s/H_a, is 2.0, 1.0 (homogeneous), and 0.5.

mixing ratios that decrease with height, so that $H_s/H_a > 1$. Of course, each absorber probably has a different scale height in the real atmosphere, but we assume here that they are all identical. With this approximation, we can now write the total optical depth and the single-scattering albedo as a function of the scatterer optical depth, i.e.,

$$\tau_t = \tau_s + \frac{H_a}{H_s}\left(\frac{1}{\varpi_1} - 1\right)\tau_s^{H_s/H_a} \quad (5)$$

and

$$\varpi_0 = \left[1 + \left(\frac{1}{\varpi_1} - 1\right)\tau_s^{H_s/H_a - 1}\right]^{-1}, \quad (6)$$

where ϖ_1 is the single-scattering albedo at the level where the scatterer optical depth is equal to one.

In Figure 3 we plot I/F ($\mu = \mu_0 = \cos 20°$, $\varphi - \varphi_0 = 180°$) for the cases $H_s/H_a = 0.5$ and 2.0, along with the homogeneous case, $H_s/H_a = 1.0$. Generalizing from the homogeneous case, we find that the function

$$I/F = [A \ln (1 - \varpi_1)]^{H_a/H_s} \quad (7)$$

gives a reasonable fit to the actual I/F if we have $A = -0.273$ for $H_s/H_a = 0.5$ and $A = -0.081$ for $H_s/H_a = 2.0$. These expressions are accurate to 10% in I/F for $0.05 < \varpi_1 < 0.9$ with $H_s/H_a = 2.0$, and for $0.45 < \varpi_1 < 0.9$ with $H_s/H_a = 0.5$, as determined using the same program that was used in testing the function in the homogeneous case. Using equation (7) in place of equation (4), we follow the same fitting procedure that was used in the homogeneous case.

The results of both the homogeneous and inhomogeneous models are presented and compared with previous measurements in the next section.

IV. MODEL RESULTS AND COMPARISONS

In this section we show the model spectra that result when the mixing ratios of C_2H_2, C_2H_6, C_4H_2, C_2H_4, and the amount of Lyman band emission are "floated," i.e., they are left as free parameters in the least squares fit of the data and are solved for by iteration, with $f_{NH_3} = f_{dust} = 0$. We consider the cases $H_s/H_a = 0.5$, 1.0, and 2.0. Later we will consider cases in which only $f_{NH_3} = 0$, and cases in which all the mixing ratios (including f_{NH_3} and f_{dust}) are floated.

Figure 4*a* presents the model spectra associated with the first situation, for the three cases $H_s/H_a = 0.5$, 1.0, and 2.0, along with the observed spectrum for comparison. It is apparent that the "continuum level" (i.e., variations on a scale of $\gtrsim 50$ Å) are extremely well accounted for by the least squares fitting process. Variations on a scale of $\lesssim 20$ Å are much harder to fit. This is due to uncertainties in the fine structure of both the solar spectrum and the cross sections used, as well as the noise in the data. Although all the models give similar results, we distinguish the best from the worst by their ability to fit these small scale variations. For instance, it may be seen that the fit for the $H_s/H_a = 2.0$ case is poor above 1700 Å, and the fit for the $H_s/H_a = 0.5$ case deteriorates below 1600 Å and has too much contrast, i.e., peak to valley amplitude. On a "quality of fit" scale from 1 (poor) to 5 (good), we would assign a 4 to the $H_s/H_a = 1.0$ case, a 3 to the $H_s/H_a = 2.0$ case, and a 2 to the $H_s/H_a = 0.5$ case.

Figure 4*b* shows how the comparison for the three cases of Figure 4*a* look in terms of the reflectivities p. The observed p is that of Figure 1*b* and is obtained by dividing the observed $F_\oplus$ by the properly scaled solar flux, then smoothing this by the instrument function. The models are just the calculated values of p smoothed by the instrument function. There is a strong anticorrelation between the models and the data from 1640 Å to 1670 Å. This is caused by artifacts of the solar C I emission feature at 1657 Å. These artifacts could be the source of the claim by Clarke, Moos, and Feldman (1982) of a C I emission feature on Jupiter. Another reason we choose to model $F_\oplus$ instead of p is that the curves in Figure 4*b* give a misleading impression of the signal-to-noise ratio of the data, which of course actually increases strongly towards the long wavelength end of the spectrum.

In Figure 5 we show the mixing ratio profiles derived for the three cases of Figures 4*a* and 4*b*. Profiles with negative slopes, vertical lines, and positive slopes correspond to the cases $H_s/H_a = 2.0$, $H_s/H_a = 1.0$, and $H_s/H_a = 0.5$, respectively. Dashed lines are used for $f_{C_2H_4}$ profiles to distinguish them from $f_{C_4H_2}$ profiles. The significance of the error bars that are plotted at the intersection regions of the profiles is discussed below. For the absorbing gases, all three profiles intersect at a pressure of ~3–10 mbar, so this appears to be the least model-dependent region to assign the calculated homogeneous mixing ratio. The physical reason for this is illustrated in Figure 6. This figure shows the contribution to the reflectivity as a function of τ_t, i.e., it is the source function weighted by $e^{-\tau/\mu}$. The source function is composed of a term due to the scattering of diffuse flux and a term due to the first scattering of attenuated solar UV. The cases $H_s/H_a = 0.5$, 1.0, and 2.0 are presented, and it is seen that in each case a large contribution to the intensity comes from above $\tau_t = 0.5$. The short dashes on each curve represent the level at which one-half the total reflectivity (~0.15) is attained. The pressures that correspond to the optical depths at a wavelength of 1650 Å are also shown in the figure.

To see the effect due to dust and NH_3, we calculate spectra for the three H_s/H_a ratios in which (1) all the mixing ratios are floated, and in which (2) only f_{NH_3} is set equal to zero. These modifications do not affect the derived hydrocarbon mixing ratios by much, although both NH_3 and dust help improve the fits for the case $H_s/H_a = 0.5$ by lowering the contrast in the region above 1700 Å. The NH_3 accomplishes this by virtue of having its absorption bands ~180° out of phase with those of C_2H_2 in this spectral region, while the dust manages the same effect by adding continuum absorption and additional scattering.

The results for all nine models are presented in Table 1. We also list an index representing the quality of fit to

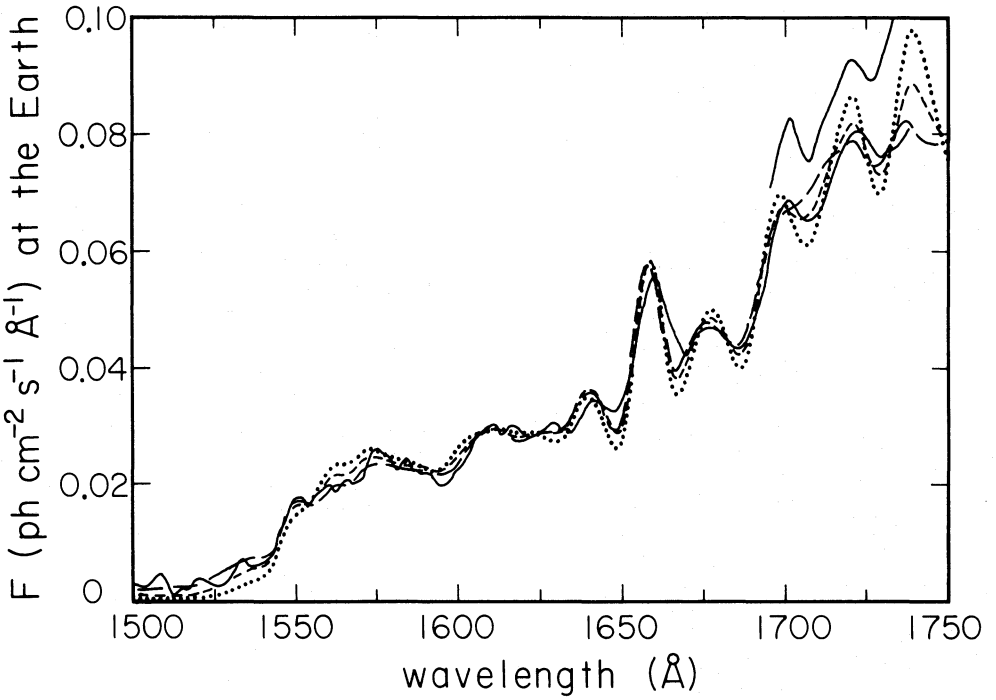

FIG. 4*a*

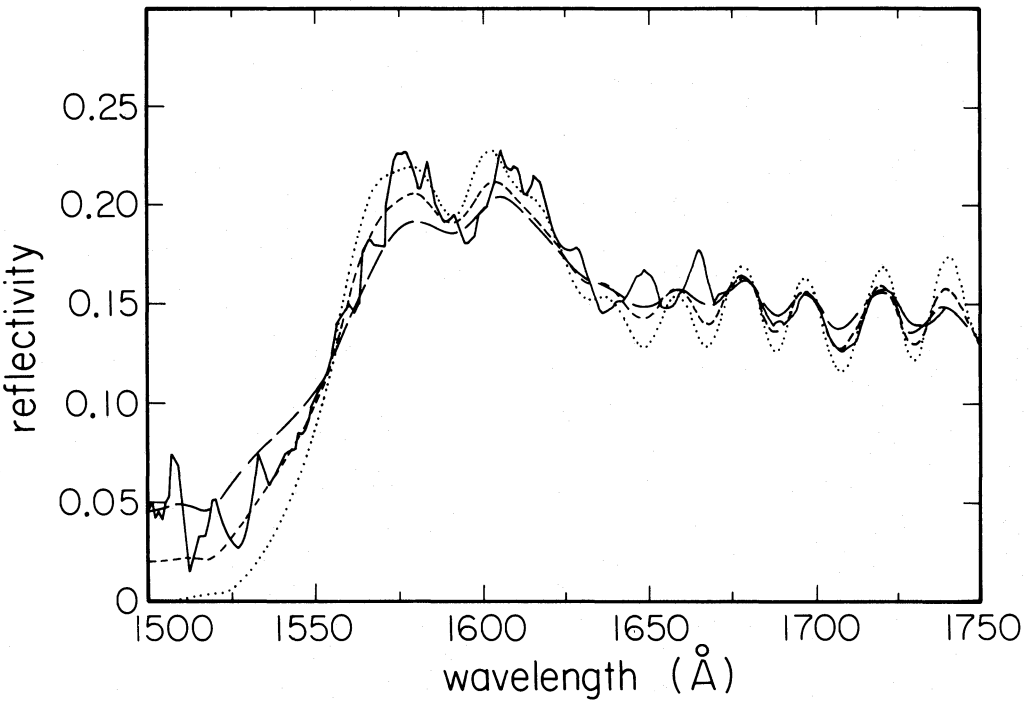

FIG. 4*b*

FIG. 4.—(*a*) *Solid line;* observed *IUE* spectra, as shown in Fig. 1*a*. *Dotted line;* model spectrum 1 ($H_s/H_s = 0.5$). *Short dashed line;* model spectrum 2 ($H_s/H_a = 1.0$). *Long dashed line;* model spectrum 3 ($H_s/H_a = 2.0$). (*b*) *Solid line;* observed *IUE* reflectivity, as shown in Fig. 1*b*. *Dotted line;* model 1 reflectivity ($H_s/H_a = 0.5$). *Short dashed line;* model 2 reflectivity ($H_s/H_a = 1.0$). *Long dashed line;* model 3 reflectivity ($H_s/H_a = 2.0$).

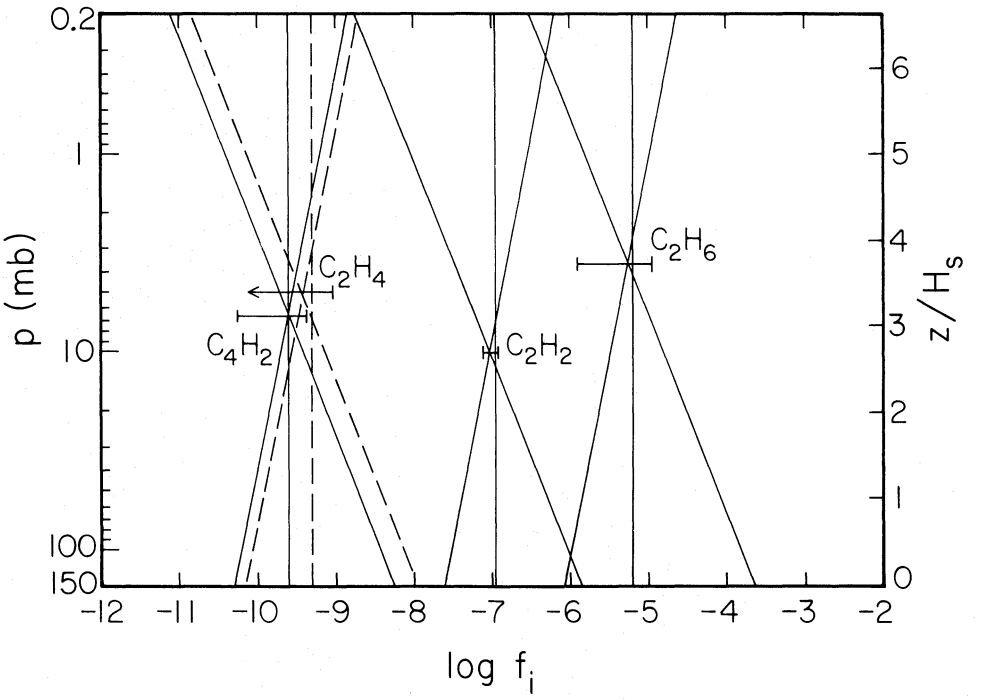

FIG. 5.—Mixing ratios of the absorbing gases for the three cases of Fig. 4 plotted against pressure and altitude (as measured in atmospheric scale heights above the tropopause). Negative slopes correspond to $H_s/H_a = 2.0$, vertical lines to $H_s/H_a = 1.0$, and positive slopes to $H_s/H_a = 0.5$. The lines for C_2H_4 are dashed to distinguish them from those for C_4H_2. The error bars plotted at the intersection regions are taken from Table 1.

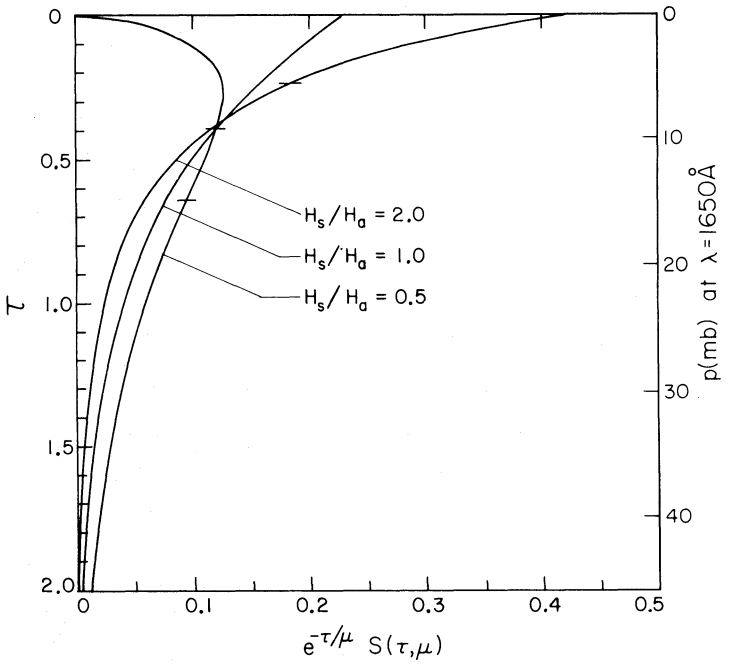

FIG. 6.—The attenuated source function (with $\mu = \cos 20°$) plotted against τ for the cases $H_s/H_a = 2.0$, 1.0, and 0.5. The backscattered intensity ($\sim$0.15) is given by the area under each curve. The horizontal dashes on each curve mark the optical depth at which one-half the backscattered reflectivity is reached.

TABLE 1

ABSORBER MIXING RATIOS AT $P = 10$ MILLIBARS AND H_2 LYMAN BAND DAYGLOW INTENSITIES DERIVED FROM LEAST SQUARES FIT

Model	H_s/H_a	Quality	$f_{C_2H_2} \times 10^6$	$f_{C_2H_6} \times 10^6$	$f_{C_4H_2} \times 10^{10}$	$f_{C_2H_4} \times 10^{10}$	$f_{dust} \times 10^{10}$	$f_{NH_3} \times 10^9$	$I_{dayglow}$ (kR)
1	0.5	2	9.4 ± 0.9	3.2 ± 2.4	2.0 ± 1.4	$2.8^{+3.3}_{-2.8}$	...	...	$0.7^{+3.3}_{-0.7}$
2	1.0	4	11 ± 1	6.5 ± 5.1	2.6 ± 1.8	4.9 ± 4.0	...	...	$1.0^{+2.6}_{-1.0}$
3	2.0	3	9.1 ± 1.5	15 ± 12	3.7 ± 2.9	7.0 ± 5.4	...	...	$16^{+2.4}_{-1.6}$
4	0.5	2	8.7 ± 0.9	3.0 ± 2.4	1.8 ± 1.1	$1.6^{+2.0}_{-1.6}$	2.3 ± 1.4	...	$0.4^{+3.5}_{-0.4}$
5	1.0	4	10 ± 1	6.6 ± 4.7	2.9 ± 2.1	$3.3^{+4.2}_{-3.3}$	1.2 ± 1.2	...	$1.5^{+3.0}_{-1.5}$
6	2.0	3	8.1 ± 1.5	14 ± 12	3.3 ± 3.0	6.6 ± 5.7	0.24 ± 0.17	...	$1.7^{+2.7}_{-1.7}$
7	0.5	4	5.9 ± 0.8	2.7 ± 2.0	1.3 ± 1.0	$2.3^{+3.3}_{-2.3}$	4.8 ± 1.0	$2.0^{+5.0}_{-2.0}$	$1.7^{+2.8}_{-1.7}$
8	1.0	4	10 ± 1	6.6 ± 5.3	2.9 ± 2.0	$3.9^{+4.9}_{-3.9}$	$1.0^{+1.4}_{-1.0}$	$4.2^{+6.7}_{-4.2}$	$1.4^{+2.4}_{-1.4}$
9	2.0	3	7.9 ± 1.6	14 ± 14	3.1 ± 2.4	$7.2^{+8.0}_{-7.2}$	0.63 ± 0.24	9^{+20}_{-9}	$1.7^{+2.6}_{-1.7}$

small-scale variations. It is seen that all the models give fairly similar results. The error bars represent 99% nonlinear confidence level bounds and take into account that we really only have $240/9.6 = 25$ independent data points. On this basis, we can only give upper limits to the mixing ratios of C_2H_4, dust, NH_3, and the dayglow intensity. Surprisingly, it seems that some C_4H_2 is necessary to obtain a good fit. We hold back from claiming a detection since there could be other absorbers not considered here that produce a similar effect. For that matter, the absorption spectra of the dust could possibly have a similar structure to that of C_4H_2 at these short wavelengths. Confirmation of C_4H_2 on Jupiter would require a less ambiguous detection, perhaps of the narrow infrared emission bands at 220 or 628 cm^{-1}.

To show the relative contributions of the absorbers at different wavelengths, we show in Figure 7 the optical depth of each absorber as a function of wavelength at a pressure of 10 mbar. Here we have used the mixing ratios derived for model 8, the homogeneous case ($H_s/H_a = 1.0$) with all mixing ratios floated (including f_{NH_3} and f_{dust}). This model was chosen because it gives upper limits to f_{dust} and f_{NH_3}. As can be seen from Table 1, choosing model 2 or model 5 would not significantly change the results. It is apparent from this figure that C_2H_6 is most important for the spectral shape below 1560 Å and C_2H_2 is most important above

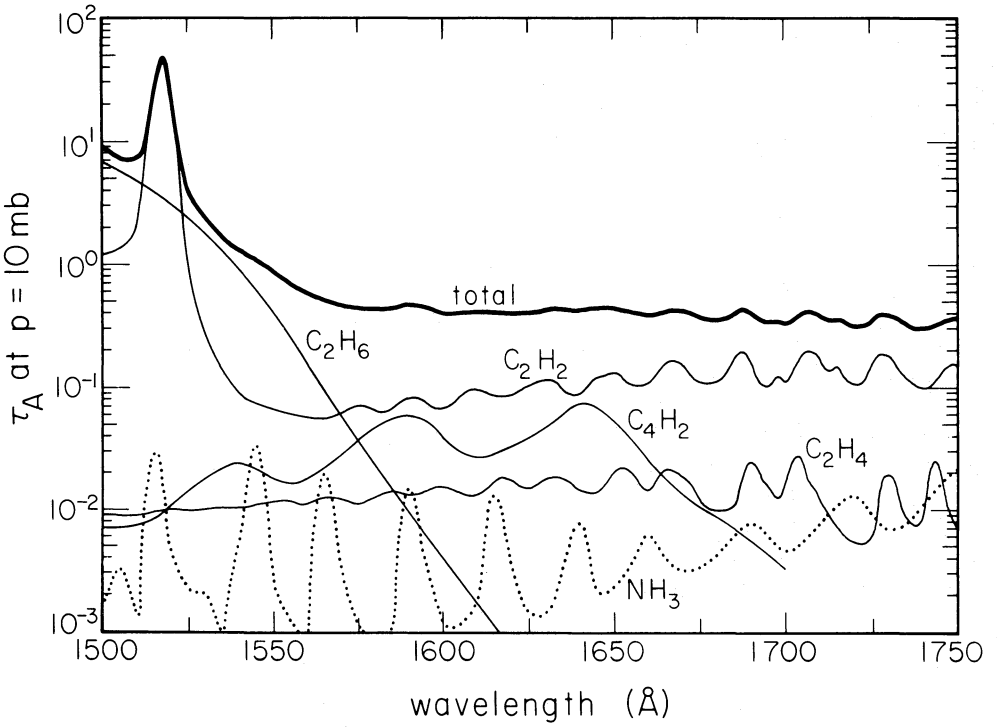

FIG. 7.—The wavelength dependence of the total optical depth and the individual absorber optical depths for C_2H_2, C_2H_6, C_4H_2, C_2H_4, and NH_3, at the level $P = 10$ mb. The mixing ratios used are taken from Table 1, model 8.

~1640 Å. The minor absorber C_4H_2 plays a relatively important role between 1580 Å and 1650 Å. The minor absorber C_2H_4, however, has bands that overlap those of C_2H_2 in this spectral region, making it clear why only an upper limit for $f_{C_2H_4}$ was obtained. NH_3 plays almost no role in this spectra, and the effect of dust is negligible. The total absorption optical depth at 10 mbar is seen to be mostly ~0.5, consistent with the results of Figures 5 and 6.

The ratio $f_{C_2H_6}/f_{C_2H_2}$ we get is 66 ± 53. This ratio is important for photochemical models of the upper atmosphere of Jupiter. The IRIS instrument on *Voyager 1* and *Voyager 2* observed C_2H_2 and C_2H_6 on Jupiter, and for the North Equatorial Belt found $f_{C_2H_2} = 3 \times 10^{-8}$ and $f_{C_2H_6} = 5 \times 10^{-6}$ at pressure level of ~15–90 mbar (Maguire 1981). In Figure 8 we plot our estimated mixing ratios and their errors, both in mixing ratio and in pressure, along with the IRIS values for C_2H_2 and C_2H_6. To the best we can determine, it appears that C_2H_6 is well mixed. However, $f_{C_2H_2}$ appears to increase with decreasing pressure, consistent with a C_2H_2 scale height equal to twice the atmospheric scale height. From Figure 8 we also conclude that while the mixing ratio obtained in model 8 for $f_{C_2H_2}$ still applies at 10 mbar, the mixing ratios for the other components now apply at different pressure levels, from ~40 mbar for dust to ~3 mbar for C_2H_6.

A value for H_s/H_a of 0.5 is also consistent with the *IUE* observations in another way. Clarke, Moos, and Feldman (1982) observed limb-darkening in a north-south scan of Jupiter in the spectral regions 1600–1650 Å, 1700–1750 Å, 1800–1850 Å, and 1900–1950 Å. In all these regions C_2H_2 is the major absorber. They found that in all cases the limb-darkening followed a roughly cosine dependence. For a backscattered reflectivity in the range of 0.15, as applies to this spectral region, there would be very little limb-darkening for a homogeneous atmosphere. Limb-darkening profiles for the cases $H_s/H_a = 0.5$, 1.0, and 2.0 are displayed in Figure 9 for values of $I/F \sim 0.15$ at $\mu = \mu_0 = 1.0$. It is seen that for $H_s/H_a = 0.5$ the dependence is most cosine-like, in agreement with the result of the IRIS comparison. However, this same cosine dependence could also be obtained if the mixing ratio of C_2H_2 generally increases from the equator toward the poles. For example, if the atmosphere were vertically homogeneous and the single-scattering albedo were to vary with latitude such that $\varpi_0 \approx 0.6$ cos (latitude), the limb-darkening would be approximately cosine. So although we favor the inhomogeneous atmosphere with $H_s/H_a = 0.5$, we cannot rule out other possibilities. The upper limit derived for the Lyman band emission, 1.4 ± 2.4 kR is consistent with the 2.8 ± 1.0 kR observed by the UVS experiment on *Voyager 1* and *Voyager 2* (Broadfoot *et al.* 1981) for the total Werner and Lyman band emission.

V. CONCLUSIONS

From our analysis of the reflected spectrum of Jupiter from 1500 Å to 1740 Å, we have obtained mixing ratios for C_2H_2, C_2H_6, C_4H_2, and upper limits on the mixing ratios of C_2H_4, NH_3, and dust in the Jovian atmosphere at ~10 mbar. It is possible that there is an appreciable amount of haze affecting the reflection spectrum, since very good model fits are obtained when dust is included.

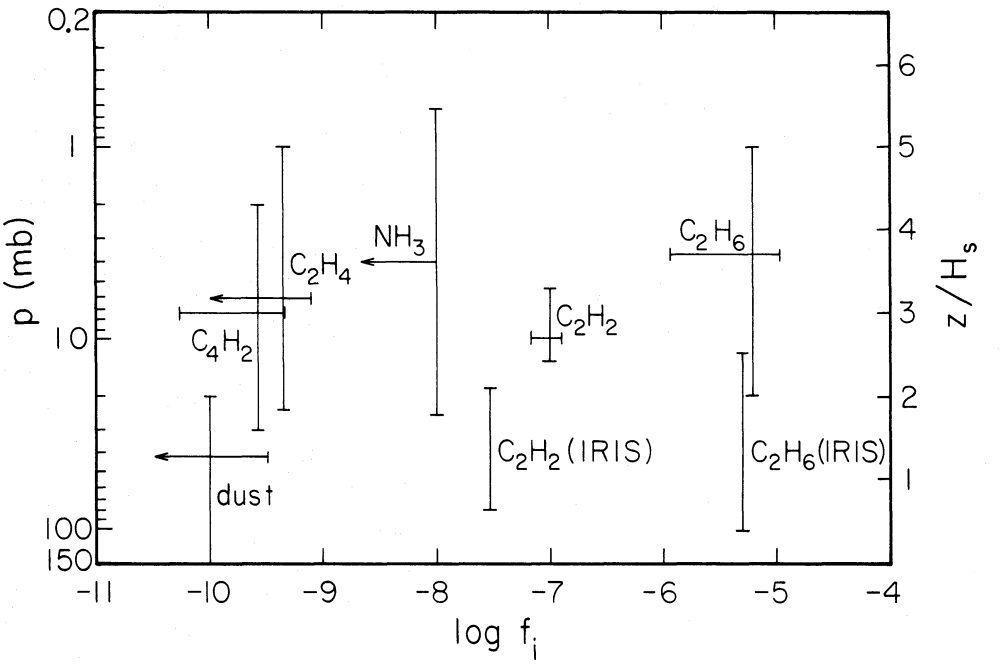

FIG. 8.—The mixing ratios and upper limits to mixing ratios derived in this study. The horizontal error bars from Table 1 and the vertical error bars are obtained from the dimensions of the intersection regions (see Fig. 5). Also shown are the values obtained by IRIS experiment on *Voyager 1* and *Voyager 2*.

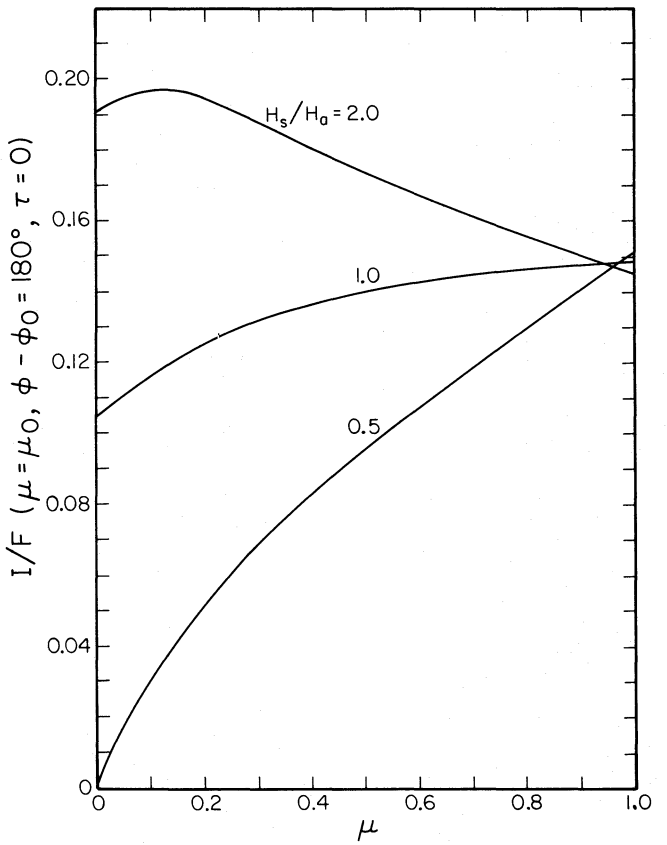

FIG. 9.—Limb darkening curves for the cases $H_s/H_a = 2.0$, 1.0, and 0.5 with I/F ($\mu = \mu_0 = \cos 20°$, $\varphi - \varphi_0 = 180°$) approximately equal to 0.15.

The scale height of C_2H_2 in this region is ~2 times the scale height of bulk atmosphere, while it appears that C_2H_6 may be well mixed. To improve on these results it will be necessary to obtain limb profiles in not only a north-south direction, as has been done by Clarke, Moos, and Feldman (1982), but also in an east-west direction. High-quality measurements of this type would probably allow the determination of the scale height of each individual absorber.

We obtain a marginal value of $1.4^{+2.4}_{-1.4}$ kR for the H_2 Lyman band dayglow emission. The uncertainty is large because most of the spectrum we are modeling is due to reflected light. If there were enough signal to model below 1525 Å we could obtain a much better result. Our value is consistent, however, with the 2.8 ± 1.0 kR observed by the UVS experiment on *Voyager 1* and *Voyager 2* (Broadfoot *et al.* 1981) for the total Werner and Lyman band dayglow emission.

We would like to thank M. Allen, J. Clarke, W. Maguire, R. Panek, M. Summers, and an anonymous reviewer for helpful comments and discussions. This research was supported by NASA grant NSG-7376 of the Planetary Atmosphere Program. This is contribution number 3646 of the Division of Geological and Planetary Sciences, California Institute of Technology.

REFERENCES

Broadfoot, A. L., *et al.* 1981, *J. Geophys. Res.*, **86**, 8259.
Clarke, J. T., Moos, H. W., and Feldman, P. D. 1982, *Ap. J.*, **255**, 806.
Ford, A. L., and Browne, J. C. 1973, *Atomic Data*, **5**, 305.
Gladstone, G. R. 1982, *J. Quant. Spectros. Rad. Trans.*, **27**, 545.
Maguire, W. 1981, private communication.
Mount, G. H., and Moos, H. W. 1978, *Ap. J.* (*Letters*), **224**, L35.
Mount, G. H., Rottman, G. J., and Timothy, J. G. 1980, *J. Geophys. Res.*, **85**, 4271.
Nakayama, T., and Watanabe, K. 1964, *J. Chem. Phys.*, **40**, 558.
Okabe, H. 1981, *J. Chem. Phys.*, **75**, 2772.
Panek, R. J. 1981, private communication.
Sato, M., and Hansen, J. E. 1979, *J. Atmos. Sci.*, **36**, 1133.
Watanabe, K. 1954, *J. Chem. Phys.*, **22**, 1564.
West, R. A. 1981, *Geophys. Res. Letters*, **8**, 847.
Yung, Y. L., Gladstone, G. R., Chang, K. M., Ajello, J. M., and Srivastava, S. K. 1982, *Ap. J.* (*Letters*), **254**, L65.
Zelikoff, M., and Watanabe, K. 1953, *J. Opt. Soc. Am.*, **43**, 756.

G. RANDALL GLADSTONE: Department of Earth and Atmospheric Science, York University, Toronto, Canada, M3J 1P3

YUK L. YUNG: Division of Geological and Planetary Sciences, California Institute of Technology, Pasadena, CA 91125